Research Article

Nano Research
2020, 13(4): 1060–1064

ISSN 1998-0124 CN 11-5974/O4
https://doi.org/10.1007/s12274-020-2744-6

Moiré patterns arising from bilayer graphone/graphene superlattice

Hu Li[1,2] (✉), Raffaello Papadakis[3], Tanveer Hussain[4], Amir Karton[4], and Jiangwei Liu[1] (✉)

[1] *Key Laboratory of High Efficiency and Clean Mechanical Manufacture, School of Mechanical Engineering, Shandong University, Jinan 250061, China*
[2] *School of Electrical and Electronic Engineering, University of Manchester, M13 9PL Manchester, UK*
[3] *Department of Chemistry, Ångström Laboratory, Uppsala University, 75 121 Uppsala, Sweden*
[4] *School of Molecular Sciences, University of Western Australia, WA6009 Perth, Australia*

Received: 2 October 2019 / **Revised:** 12 February 2020 / **Accepted:** 4 March 2020

ABSTRACT

Moiré patterns from two-dimensional (2D) graphene heterostructures assembled via van der Waals interactions have sparked considerable interests in physics with the purpose to tailor the electronic properties of graphene. Here we report for the first time the observation of moiré patterns arising from a bilayer graphone/graphene superlattice produced through direct single-sided hydrogenation of a bilayer graphene on substrate. Compared to pristine graphene, the bilayer superlattice exhibits a rippled surface and two types of moiré patterns are observed: triangular and linear moiré patterns with the periodicities of 11 nm and 8–9 nm, respectively. These moiré patterns are revealed from atomic force microscopy and further confirmed by following fast Fourier transform (FFT) analysis. Density functional theory (DFT) calculations are also performed and the optimized lattice constants of bilayer superlattice heterostructure are in line with our experimental analysis. These findings show that well-defined triangular and linear periodic potentials can be introduced into the graphene system through the single-sided hydrogenation and also open a route towards the tailoring of electronic properties of graphene by various moiré potentials.

KEYWORDS

Moiré patterns, graphone/graphene superlattice, atomic force microscopy, triangular pattern, linear pattern

1 Introduction

In the last two decades there has been a tremendous interest in graphene primarily because of its unique physical and chemical properties, and a significant portion of the performed and ongoing research on graphene aims at tailoring its properties so as to render the material appropriate in a vast number of new technological applications [1–8]. A milestone in this endeavour is tailoring its electronic properties through periodic potentials which create secondary Dirac points and affect the local density of states of graphene. This effect can be achieved through the formation of moiré interference between two graphene layers or a graphene layer and a crystalline substrate [9–12]. Yankowitz et al. reported on the development of superlattice Dirac points in graphene on a crystalline hexagonal boron nitride substrate [13]. In a similar fashion, Yang et al. observed moiré patterns when investigating the epitaxial growth of graphene on the same substrate with a clear evidence of superlattice Dirac points [14]. Moiré superlattices have been also developed in graphene utilizing a variety of metal substrates [15]. The choice of the metal substrate has been shown to largely influence the band structure of graphene and more specifically, metal substrates such as Ni [16] or Ru [17], which strongly interact with a graphene layer, can induce sizable modification on the band structure of graphene. Metal substrates exhibiting weaker interactions with graphene such as Ir or Pt preserve the linear dispersion feature of graphene [18, 19]. Generally, the lattice mismatch in moiré superlattices of graphene on a crystalline substrate constitutes a key parameter influencing the energy at which the superlattice Dirac point appears. Similar observations have also been made in case of twisted bilayer graphene, where firstly Li et al. [20] and later Brihuega et al. [21] observed the emergence of van Hove singularities and their dependence on the rotation angle between the two graphene layers. Similarly to the twisted bilayer graphene, graphene derivatives, e.g. fluorographene (CF), graphane (CH) and graphone (C_2H), due to their lattice constant being slightly different from that of graphene, have the potential to form moiré superlattices when they are well aligned on top of the monolayer graphene. However, after synthesis, the obtained graphene derivatives always show a rippled surface [22], so that the transferred graphene derivative layer cannot atomically lock to the bottom flat graphene to form the moiré superlattice. Therefore, to the best of our knowledge, there is no report on the formation of moiré superlattices involving a graphene layer and a graphene derivative layer such as hydrogenated graphene up to date.

In this work we report the formation of triangular and linear moiré patterns arising from a bilayer graphone/graphene superlattice produced through the direct hydrogenation of a pristine bilayer graphene, leading to the hydrogenation of the upper layer but leaving the lower graphene layer intact. The formation of as described moiré patterns from the bilayer graphone/graphene superlattice is confirmed by atomic force microscopy (AFM) measurements and corresponding fast Fourier transform analysis, and is further supported from the density functional theory (DFT) calculations.

Address correspondence to Hu Li, Hu.Li@manchester.ac.uk; Jiangwei Liu, Jiangwei.Liu@sdu.edu.cn

2 Experimental

2.1 Direct synthesis of graphone/graphene bi-layer superlattice

In this work, bilayer graphene was prepared by mechanical exfoliation from the highly oriented pyrolytic graphite (HOPG) onto the SiO_2 (300 nm)/Si substrate. It was first locally positioned by light optical microscopy and further confirmed by means of Raman spectroscopy (XploRA Plus Confocal Raman Microscope, Horiba). Prior to the mechanical exfoliation, scanning tunnelling microscopy (STM) was performed on the HOPG samples to investigate the intrinsic stacking order of the graphene layers by using a Bruker Multimode 8 AFM in the STM mode. The hydrogenation of the top layer graphene in the bilayer structure was conducted by exposure of the bilayer graphene to atomic hydrogens produced via cracking of molecular H_2 by plasmas [5]. In the experiment, an electrical arc is formed between two aluminium electrodes under the input voltage of 25 kV, power of 15 W and a frequency of 160 Hz under a low chamber pressure of 0.1 mbar. To minimize the possible structural damage from the energetic particles, the graphene sample is positioned away from the discharge zone and a total hydrogenation time of 30 minutes is employed in the process. The previous study has shown that the substrate normally prevents the atomic hydrogen diffusion along the graphene-SiO_2 interface, leading to the single-sided hydrogenation of graphene on the substrate [5, 22–24]. Therefore in our case, the plasma method for hydrogenation on bilayer graphene can only result in a graphone (single-sided hydrogenated graphene)/graphene superlattice. Before and after the hydrogenation, Raman spectroscopy was performed on the bilayer graphene sample to investigate the structure modification, and the generated moiré patterns were revealed from a Bruker Icon AFM under peakforce quantitative nanomechanical mapping (PF-QNM) mode by using a silicon AFM tip.

2.2 Density functional theory calculations

We performed spin-polarized first principles calculations based on DFT by using Vienna Ab initio Simulation Package (VASP) [25–27]. Generalized gradient approximation (GGA) was used to tackle the exchange-correlation functional whereas projector-augmented wave method (PAW) was adopted to deal with the electron-ion interactions [28, 29]. Van der Waals correction (DFT-D3) to our DFT calculations was further used in order to counterbalance the underestimation of GGA in the calculation of binding interactions [30]. For the plane wave basis set, we used cut-off energy of 500 eV. For both graphene and graphone monolayers, 3 × 3 × 1 supercells were used having 18 (18 C) and 27 (18 C, 9 H) atoms, respectively. To nullify the possible interactions between the periodic images, a vacuum space of 18 Å was introduced in the vertical *z*-direction. For the Brillouin zone sampling, a mesh of 5 × 5 × 1 for structural optimization and 15 × 15 × 1 for the calculation of density of states under Monkhorst-Pack scheme were used [31]. We used a convergence and force criteria of 10^{-6} eV and 0.01eV/Å, respectively.

3 Results and discussion

The initial stacking order of the starting material is of great importance for the investigation and simulation of the generated moiré patterns. Therefore, STM measurements were first conducted on the HOPG prior to the mechanical exfoliation. Figure 1(a) shows the atomic resolution STM image of graphite, which depicts a highly intact lattice structure and long-range triangular lattice with a periodicity of ≈ 0.25 nm. This structure corresponds well with the Bernal stacking order of the graphite [7, 32]. The bilayer graphene flake was prepared by mechanical exfoliation from the HOPG on the SiO_2 (300 nm)/Si substrate. Figure 1(b) shows the optical microscopy image of the bilayer graphene, where position A and B denote the areas of bilayer graphene and monolayer graphene, respectively. Before and after hydrogenation, the Raman spectroscopy measurements were performed to understand the structure modifications, as shown in Fig. 1(c). In pristine monolayer and bilayer graphene, prominent 2D peak (at ~ 2,680 cm^{-1}) is observed in both Raman spectra and the intensity ratios between the 2D peak and G peak (at ~ 1,580 cm^{-1}) are found to be 3:1 and 1:1, respectively, corresponding well with the Raman fingerprint signatures of the monolayer and bilayer graphene. The D peak (at ~ 1,350 cm^{-1}) indicating the defect level is found to be negligible in both spectra, which implies that the graphene samples are high-quality and defect-free. After hydrogenation, an intense and sharp D peaks are both observed in monolayer and bilayer graphene samples, which is mainly attributed to the broken translational symmetry of sp^2 carbon–carbon bonds due to the formation of C–H bonds in graphene [5, 33, 34]. In the hydrogenated monolayer graphene, the intensity ratio of the D peak and G peak is found to be I_D/I_G = 1.31, which is in line with the report on the saturated single-sided hydrogenation of graphene [22, 35]. As for the hydrogenated bilayer graphene, the I_D/I_G = 0.68 is obtained from the spectrum, indicating that the surface is only partially hydrogenated. This observation actually has been noticed experimental and it is attributed to the higher rigidity of bilayer, which suppresses its ripples which is energy favourable through hydrogen fixation [22, 36, 37].

Theoretically, graphene derivatives, e.g. graphane (CH), graphone (C_2H) and fluorographene (CF), can potentially form moiré superlattices through aligning well with monolayer graphene due to their similar hexagonal lattice structure and small lattice mismatch. However, after synthesis, the obtained graphene derivatives always show a rippled surface which facilitates the functionalization, and after transferring onto

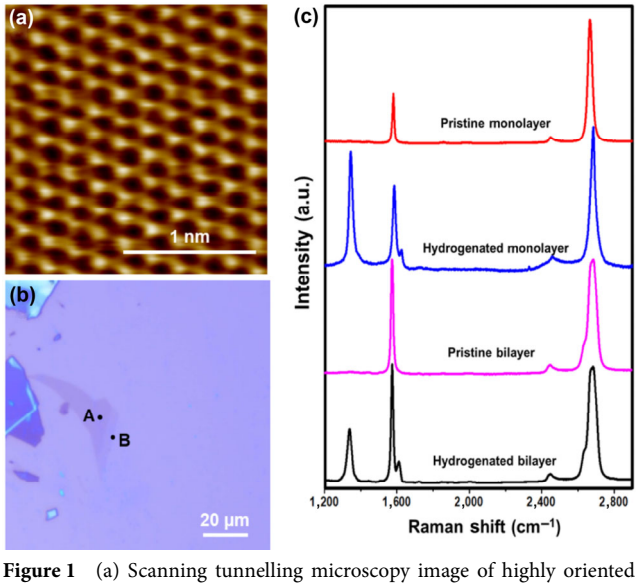

Figure 1 (a) Scanning tunnelling microscopy image of highly oriented pyrolytic graphite, indicating the Bernal stacking order of the graphene layers. (b) Light optical image of the exfoliated graphene. Area A is the bilayer graphene and area B is the monolayer graphene. (c) Raman spectrum comparison of the monolayer graphene and bilayer graphene before and after the hydrogenation process.

planar monolayer graphene, the graphene derivative layer thus is difficult to atomically lock to the flat graphene layer to form the moiré superlattice. To address this concern, our strategy in this work is to directly hydrogenate the topmost layer in the exfoliated bilayer graphene and achieve the C_2H/graphene superlattice structure. Conventional characterization technique, e.g. scanning tunnelling microscopy, is not feasible for the observation of the moiré patterns due to the electrical insulating character of the substrate SiO_2, therefore, AFM is mainly employed in our work. When performing the AFM imaging on our bilayer graphene surface, a significant morphology modification of the bilayer graphene is the observation of the rippled surface after hydrogenation (Fig. 2(b)), while the pristine bilayer graphene always shows a planar surface (Fig. 2(a)). According to the reported work on the formation of hBN bubbles by plasma treatment [38], the rippled structure is most likely due to the atomic hydrogens moving through the bilayer graphene. Moreover, since the hydrogenation triggers a conversion of sp^2 carbon to sp^3 carbon, this process will create strains in the graphene lattice and thus also contribute to the formation of the ripples. From the image shown in Fig. 2(b), we can classify the surface into two areas: the ripple and the comparably flat areas. Zoomed-in and fine scanned AFM imaging was performed on both areas.

First of all, on the comparably flat area, there are two types of moiré patterns observed as shown in Fig. 3. Figure 3(a) shows an intact area consisting of periodically triangular order of moiré patterns which depicted a moiré wavelength (long-range periodicity) of 11 nm with 60° vector angle as indicated in the AFM image. The fast Fourier transform (FFT) of the image as shown in Fig. 3(b) further confirms the triangular periodicity of the moiré patterns as indicated. The observed superlattice possess the typical triangular moiré patterns that have been reported from the hBN/graphene superlattice [39] but with a different periodicity, which implies the successful fabrication of the graphone (C_2H)/graphene superlattice with top graphone layer atomically locked onto the bottom graphene layer. Figure 3(c) shows another pattern that is observed on the flat area as well. Even if there are some potential lines appearing in the image, it is difficult to get clear moiré patterns due to the much less periodicity compared to the AFM image shown in Fig. 3(a). It is noted that both of the pattern sites are atomically flat with the measured surface roughness less than 0.3 Å, which implies that there is no significant damage that happened here. Therefore, we mainly attribute the blurred patterns to the insufficient hydrogenations that thus cannot generate uniform hexagonal lattice on the upmost layer of graphene. To the best of our knowledge, our result is the first experimental observation of the bilayer moiré superlattice in the graphene derivative/graphene system and the fabricated graphone/graphene superlattice will be a new platform for

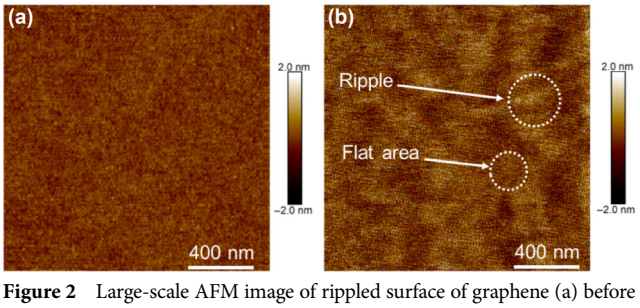

Figure 2 Large-scale AFM image of rippled surface of graphene (a) before and (b) after hydrogenation. The doted circles denote the positions of the ripple and flat areas, respectively.

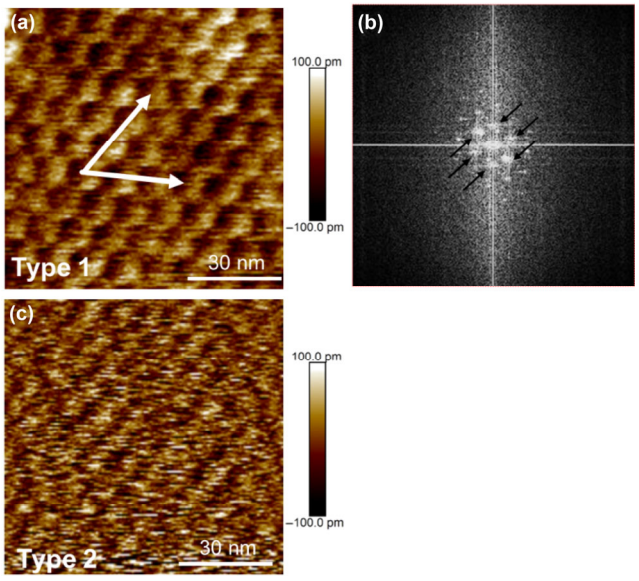

Figure 3 (a) Zoomed-in AFM image of the type 1 moiré pattern. (b) Fast Fourier transform of the type 1 scan area, which confirms the triangular periodicity as indications. (c) Zoomed-in AFM image of type 2 pattern with less order.

the investigation of the electronic properties of graphene, in addition to previously reported and dominating graphene/hBN system.

Through the work of Tang [39], the moiré wavelength λ in bilayers is closely related to the lattice mismatch δ, which can be quantitatively extracted from a simple equation: $\lambda = (1-\delta)a/\delta$, where a is the graphene lattice constant as shown in Fig. 3(a) and the lattice mismatch can be expressed as: $\delta = (b-a)/a \times 100\%$, where b is the lattice constant of top layer graphone as shown in Fig. 3(b). As a consequence, we have plotted the moiré wavelength as a function of the lattice mismatch in Fig. 3(c) and it is concluded that the moiré wavelength of 11 nm corresponds to a lattice mismatch of ~ 2.2%. To further confirm our result, we have simulated the moiré patterns arising from bilayers with 2.2% lattice mismatch and initial Bernal stacking as shown in Fig. 3(d). The resulting pattern is quite similar and matches well with our experimental observations. It has been reported that, apart from the C_2H chair configuration, the graphone also has a C_2H boat configuration [40, 41] (Fig. S1(a) in the ESM).To investigate the possible generated moiré pattern from the C_2H boat/graphene superlattices, we also carried out the simulations that can be found in Fig. S1(b) (in the ESM), which shows a rectangular moiré pattern that is distinguished from our observed triangular moiré pattern.

As for the ripple area denoted in Fig. 2(b), an anomalous linear moiré pattern is observed as shown in Fig. 5(a). This linear moiré pattern with the periodicity of 8–9 nm is confirmed from the FFT and cross-profile measurements as shown in Figs. 5(b) and 5(c), respectively. The formation mechanism of such linear moiré pattern is still unknown to us and one possible explanation could be that, at the rippled site, the upmost graphone layer is slightly stretched (strained, see supporting information), leading to a small mismatch along one direction and thus generate the linear moiré pattern (we also simulate this case and the obtained pattern can be found in Fig. S2 (in he ESM)). But more detailed studies need to be carried out to better investigate the mechanism of such anomalous linear moiré pattern.

DFT calculations are also performed to better understand the structure of the graphone/graphene superlattice (Fig. 6).

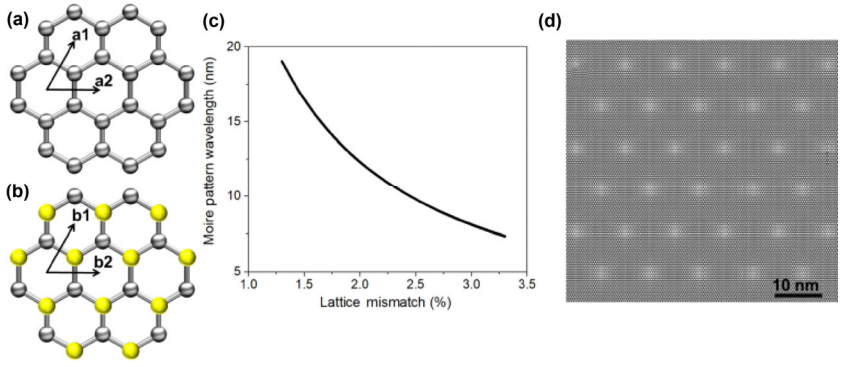

Figure 4 Schematic illustrations of the (a) graphene and (b) graphone (C_2H chair configuration) with lattice vectors. The silver and yellow spheres denote the C and H atoms, respectively. (c) The calculated moiré pattern wavelength as a function of lattice mismatch. (d) Simulated moiré patterns of the graphone (C_2H chair configuration)/graphene superlattice with a mismatch of 2.2%, which matches well with the calculation of a moiré wavelength of 11 nm.

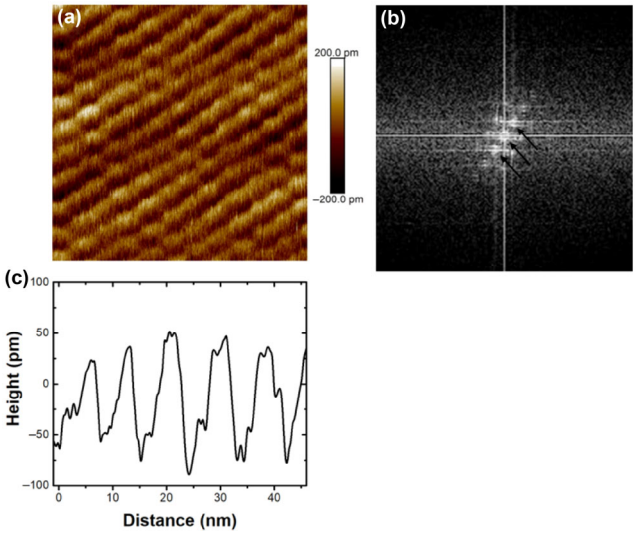

Figure 5 (a) Zoomed-in AFM image of the ripple area that shows ordered line moiré patterns. (b) Fast Fourier transform of the scan area, which confirms the line periodicity. (c) Profile of the line patterns with the periodicity of 8–9 nm.

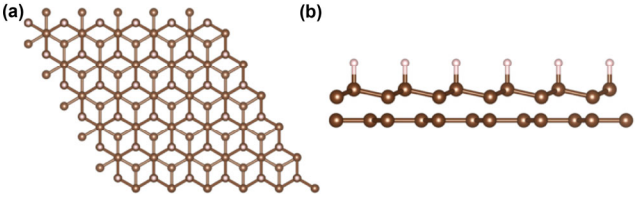

Figure 6 Top view (a) and side view (b) of the optimized structure of graphone/graphene superlattice, brown and pink balls represent C and H atoms, respectively. The optimized lattice constants, C–C (graphene), C–C (graphone) bonds lengths are found to be 1.43 and 1.51 Å, respectively, and the lattice spacing is 3.409 Å.

Through our calculations, the optimized lattice constant, C–C (graphene), C–C (graphone) bonds lengths are found to be 1.43 and 1.51 Å, respectively, which agrees with the literature [42]. Moreover, when the C–C bonds from the graphone are projected on to the bottom graphene plane, a lattice mismatch of ~ 2.3% was obtained, which matches our experimental values and calculations. Extra projected density of states (PDOS) of such heterostructure can be found in Fig. S3 in the ESM.

4 Conclusions

Herein, we report the formation of triangular and linear moiré patterns for the first time arising from a directly fabricated graphone/graphene bilayer superlattice, which is produced through single-sided hydrogenation of a bilayer graphene. The triangular moiré pattern shows a long-range periodicity of ~ 11 nm, corresponding to a 2.2% lattice mismatch between top layer graphone and bottom layer graphene, while the linear moiré patterns exhibit a periodicity of 8–9 nm. To the best of our knowledge, the newly reported moiré patterns are the first observation of the moiré patterns from the derivatised graphene bilayer superlattice. It provides a novel platform to investigate and tailor the electronic properties of the graphene and the rich physics in this remains largely unexploited.

Acknowledgements

We acknowledge the financial support from the National Natural Science Foundation of China (No. 51905306), the China Postdoctoral Science Fund (No. 2018M642650) and the Special Support for Post-doc Creative Funding of Shandong Province (No. 201902005). We are also grateful for the funding support from the University of Manchester Donator Foundation and Swedish Research Council Formas (No. 2019-01538). Dr. Chloe Holyord from National Graphene Institute, University of Manchester is gratefully acknowledged for the help with AFM measurements. Dr. Linqing Zhang and Mr. Malachy Mcgowan are greatly acknowledged for the experimental support in the sample preparation.

Electronic Supplementary Material: Supplementary material (details of more simulated moirés patterns and electronic structure of the superlattice) is available in the online version of this article at https://doi.org/10.1007/s12274-020-2744-6.

References

[1] Ponomarenko, L. A.; Gorbachev, R. V.; Yu, G. L.; Elias, D. C.; Jalil, R.; Patel, A. A,; Mishchenko, A.; Mayorov, A. S.; Woods, C. R.; Wallbank, J. R. et al. Cloning of Dirac fermions in graphene superlattices. *Nature* **2013**, *497*, 594–597.

[2] Geim, A. K. Graphene: Status and prospects. *Science* **2009**, *324*, 1530–1534.

[3] Gorbachev, R. V.; Song, J. C. W.; Yu, G. L.; Kretinin, A. V.; Withers, F.; Cao, Y.; Mishchenko, A.; Grigorieva, I. V.; Novoselov, K. S.; Levitov, L. S. et al. Detecting topological currents in graphene superlattices. *Science* **2014**, *346*, 448–451.

[4] Li, H.; Daukiya, L.; Haldar, S.; Lindblad, A.; Sanyal, B.; Eriksson, O.; Aubel, D.; Hajjar-Garreau, S.; Simon, L.; Leifer, K. Site-selective local fluorination of graphene induced by focused ion beam irradiation. *Sci. Rep.* **2016**, *6*, 19719.

[5] Liu, J. W.; Chen, S.; Papadakis, R.; Li, H. Nanoresolution patterning of hydrogenated graphene by electron beam induced C–H dissociation. *Nanotechnology* **2018**, *29*, 415304.

[6] Lundstedt, A.; Papadakis, R.; Li, H.; Han, Y. Y.; Jorner, K.; Bergman, J.; Leifer, K.; Grennberg, H.; Ottosson, H. White-light photoassisted covalent functionalization of graphene using 2-propanol. *Small Methods* **2017**, *1*, 1700214.

[7] Wang, N.; Samani, M. K.; Li, H.; Dong, L.; Zhang, Z. W.; Su, P.; Chen, S. J.; Chen, J.; Huang, S. R.; Yuan, G. J. et al. Tailoring the thermal and mechanical properties of graphene film by structural engineering. *Small* **2018**, *14*, 1801346.

[8] Li, H.; Papadakis, R.; Jafri, S. H. M.; Thersleff, T.; Michler, J.; Ottosson, H.; Leifer, K. Superior adhesion of graphene nanoscrolls. *Commun. Phys.* **2018**, *1*, 44.

[9] Kumar, R. K.; Chen, X.; Auton, G. H.; Mishchenko, A.; Bandurin, D. A.; Morozov, S. V.; Cao, Y.; Khestanova, E.; Ben Shalom, M.; Kretinin, A. V. et al. High-temperature quantum oscillations caused by recurring Bloch states in graphene superlattices. *Science* **2017**, *357*, 181–184.

[10] Cao, Y.; Fatemi, V.; Fang, S. A.; Watanabe, K.; Taniguchi, T.; Kaxiras, E.; Jarillo-Herrero, P. Unconventional superconductivity in magic-angle graphene superlattices. *Nature* **2018**, *556*, 43–50.

[11] Cao, Y.; Fatemi, V.; Demir, A.; Fang, S. A.; Tomarken, S. L.; Luo, J. Y.; Sanchez-Yamagishi, J. D.; Watanabe, K.; Taniguchi, T.; Kaxiras, E. et al. Correlated insulator behaviour at half-filling in magic-angle graphene superlattices. *Nature* **2018**, *556*, 80–84.

[12] Dean, C. R.; Wang, L.; Maher, P.; Forsythe, C.; Ghahari, F.; Gao, Y.; Katoch, J.; Ishigami, M.; Moon, P.; Koshino, M. et al. Hofstadter's butterfly and the fractal quantum Hall effect in moiré superlattices. *Nature* **2013**, *497*, 598–602.

[13] Khitrova, G.; Gibbs, H. M.; Kira, M.; Koch, S. W.; Scherer, A. Vacuum Rabi splitting in semiconductors. *Nat. Phys.* **2006**, *2*, 81–90.

[14] Yang, W.; Chen, G. R.; Shi, Z. W.; Liu, C. C.; Zhang, L. C.; Xie, G. B.; Cheng, M.; Wang, D. M.; Yang, R.; Shi, D. X. et al. Epitaxial growth of single-domain graphene on hexagonal boron nitride. *Nat. Mater.* **2013**, *12*, 792–797.

[15] Wintterlin, J.; Bocquet, M. L. Graphene on metal surfaces. *Surf. Sci.* **2009**, *603*, 1841–1852.

[16] Sutter, P.; Hybertsen, M. S.; Sadowski, J. T.; Sutter, E. Electronic structure of few-layer epitaxial graphene on Ru(0001). *Nano Lett.* **2009**, *9*, 2654–2660.

[17] Dedkov, Y. S.; Fonin, M.; Rüdiger, U.; Laubschat, C. Rashba effect in the graphene/Ni(111) system. *Phys. Rev. Lett.* **2008**, *100*, 107602.

[18] Pletikosić, I.; Kralj, M.; Pervan, P.; Brako, R.; Coraux, J.; N'Diaye, A. T,; Busse, C.; Michely, T. Dirac cones and minigaps for graphene on Ir(111). *Phys. Rev. Lett.* **2009**, *102*, 056808.

[19] Gao, M.; Pan, Y.; Huang, L.; Hu, H.; Zhang, L. Z.; Guo, H. M.; Du, S. X.; Gao, H. J. Epitaxial growth and structural property of graphene on Pt(111). *Appl. Phys. Lett.* **2011**, *98*, 033101.

[20] Li, G. H.; Luican, A.; Lopes Dos Santos, J. M. B.; Castro Neto, A. H.; Reina, A.; Kong, J.; Andrei, E. Y. Observation of Van Hove singularities in twisted graphene layers. *Nat. Phys.* **2010**, *6*, 109–113.

[21] Brihuega, I.; Mallet, P.; González-Herrero, H.; Trambly De Laissardière, G.; Ugeda, M. M.; Magaud, L.; Gómez-Rodríguez, J. M.; Ynduráin, F.; Veuillen, J. Y. Unraveling the intrinsic and robust nature of van hove singularities in twisted bilayer graphene by scanning tunneling microscopy and theoretical analysis. *Phys. Rev. Lett.* **2012**, *109*, 196802.

[22] Elias, D. C.; Nair, R. R.; Mohiuddin, T. M. G.; Morozov, S. V.; Blake, P.; Halsall, M. P.; Ferrari, A. C.; Boukhvalov, D. W.; Katsnelson, M. I.; Geim, A. K. et al. Control of Graphene's properties by reversible hydrogenation: Evidence for Graphane. *Science* **2009**, *323*, 610–613.

[23] Sessi, P.; Guest, J. R.; Bode, M.; Guisinger, N. P. Patterning graphene at the nanometer scale via hydrogen desorption. *Nano Lett.* **2009**, *9*, 4343–4347.

[24] Guisinger, N. P.; Rutter, G. M.; Crain, J. N.; First, P. N.; Stroscio, J. A. Exposure of epitaxial graphene on SiC(0001) to atomic hydrogen. *Nano Lett.* **2009**, *9*, 1462–1466.

[25] Kresse, G.; Hafner, J. *Ab initio* molecular dynamics for liquid metals. *Phys. Rev. B* **1993**, *47*, 558–561.

[26] Kresse, G.; Hafner, J. *Ab initio* molecular-dynamics simulation of the liquid-metal–amorphous-semiconductor transition in germanium. *Phys. Rev. B* **1994**, *49*, 14251–14269.

[27] Kresse, G.; Furthmüller, J. Efficient iterative schemes for *ab initio* total-energy calculations using a plane-wave basis set. *Phys. Rev. B* **1996**, *54*, 11169–11186.

[28] Perdew, J. P.; Burke, K.; Ernzerhof, M. Generalized gradient approximation made simple. *Phys. Rev. Lett.* **1996**, *77*, 3865–3868.

[29] Blöchl, P. E. Projector augmented-wave method. *Phys. Rev. B* **1994**, *50*, 17953–17979.

[30] Grimme, S. Semiempirical GGA-type density functional constructed with a long-range dispersion correction. *J. Comput. Chem.* **2006**, *27*, 1787–1799.

[31] Monkhorst, H. J.; Pack, J. D. Special points for Brillouin-zone integrations. *Phys. Rev. B* **1976**, *13*, 5188–5192.

[32] Yan, K.; Peng, H. L.; Zhou, Y.; Li, H, ; Liu, Z. F. Formation of bilayer Bernal graphene: Layer-by-layer epitaxy via chemical vapor deposition. *Nano Lett.* **2011**, *11*, 1106–1110.

[33] Ansari, R.; Mirnezhad, M.; Rouhi, H. Mechanical properties of fully hydrogenated graphene sheets. *Solid State Commun.* **2015**, *201*, 1–4.

[34] Papadakis, R.; Li, H.; Bergman, J.; Lundstedt, A.; Jorner, K.; Ayub, R.; Haldar, S.; Jahn, B. O.; Denisova, A.; Zietz, B.; Lindh, R. et al. Metal-free photochemical silylations and transfer hydrogenations of benzenoid hydrocarbons and graphene. *Nat. Commun.* **2016**, *7*, 12962.

[35] Jones, J. D.; Mahajan, K, K.; Williams, W. H.; Ecton, P. A.; Mo, Y.; Perez, J. M. Formation of graphane and partially hydrogenated graphene by electron irradiation of adsorbates on graphene. *Carbon* **2010**, *48*, 2335–2340.

[36] Meyer, J. C.; Geim, A. K.; Katsnelson, M. I.; Novoselov, K. S.; Booth, T. J.; Roth, S. The structure of suspended graphene sheets. *Nature* **2007**, *446*, 60–63.

[37] Meyer, J. C.; Geim, A. K.; Katsnelson, M. I.; Novoselov, K. S.; Obergfell, D.; Roth, S.; Girit, C.; Zettl, A. On the roughness of single- and bi-layer graphene membranes. *Solid State Commun.* **2007**, *143*, 101–109.

[38] He, L.; Wang, H. S.; Chen, L. X.; Wang, X. J.; Xie, H.; Jiang, C. X.; Li, C.; Elibol, K.; Meyer, J.; Watanabe, K. et al. Isolating hydrogen in hexagonal boron nitride bubbles by a plasma treatment. *Nat. Commun.* **2019**, *10*, 2815.

[39] Tang, S. J.; Wang, H. M.; Zhang, Y.; Li, A.; Xie, H.; Liu, X. Y.; Liu, L. Q.; Li, T. X.; Huang, F. Q.; Xie, X. M. et al. Precisely aligned graphene grown on hexagonal boron nitride by catalyst free chemical vapor deposition. *Sci. Rep.* **2013**, *3*, 2666.

[40] Yi, D.; Yang, L.; Xie, S. J.; Saxena, A. Stability of hydrogenated graphene: A first-principles study. *RSC Adv.* **2015**, *5*, 20617–20622.

[41] Averill, F. W.; Morris, J. R.; Cooper, V. R. Calculated properties of fully hydrogenated single layers of BN, BC_2N, and graphene: Graphane and its BN-containing analogues. *Phys. Rev. B* **2009**, *80*, 195411.

[42] Zhou, J.; Wang, Q.; Sun, Q.; Chen, X. S.; Kawazoe, Y.; Jena, P. Ferromagnetism in semihydrogenated graphene sheet. *Nano Lett.* **2009**, *9*, 3867–3870.